Agr. Nat. Resour. 57 (2023) 799–808

AGRICULTURE AND NATURAL RESOURCES

Journal homepage: http://anres.kasetsart.org

Research article

Simulation and optimization of centrifugal propellers for Pacific white shrimp harvesting

Songphon Thoetrattanakiat[a], Kiattisak Sangpradit[b,*]

[a] *Engineering Field of Study, Faculty of Engineering, Rajamangala University of Technology Thanyaburi, Pathum Thani 12110, Thailand*

[b] *Department of Agriculture Engineering, Faculty of Engineering, Rajamangala University of Technology, Thanyaburi, Pathum Thani 12110, Thailand*

Article Info

Article history:
Received 1 July 2023
Revised 10 August 2023
Accepted 1 September 2023
Available online 31 October 2023

Keywords:
Centrifugal pump technique,
Fluid harvesting,
Propeller design,
Shrimp harvesting methods,
White shrimp farming

Abstract

Importance of the work: Traditional shrimp harvesting methods can be improved, with one option being to investigate optimizing centrifugal pump-based white shrimp harvesting (20–29 shrimps/kg) through experimental investigations.

Objectives: To identify efficient white shrimp harvesting using a centrifugal pump technique, to evaluate five propeller designs and to analyze their forces, flow rate and pressure at varying speeds.

Materials & Methods: Five propeller designs were assessed for harvesting of white shrimp in the 20–29 shrimps/kg size range using the centrifugal pump technique. Force, flow rate and pressure were analyzed at different propeller speeds (240, 255, 270, 285 and 300 revolutions per minute, RPM) within the pump housing, considering nine positions to gauge their impact.

Results: The IM1 impeller performed well, delivering adequate flow rates. At 240 RPM, the flow rate was 138 m^3/hr, reaching 886 m^3/hr at 300 RPM. The pump pressure peaked at 161,637 Pa at 300 RPM, with nine pressure peaks on the white shrimp body, reaching 162,664 Pa at position 7. The IM1 impeller demonstrated optimal performance at 270 RPM, reaching 157,864 Pa pressure and a flow rate of 657 m^3/hr.

Main finding: Comparing the various propeller types, the IM1 impeller outperformed the other propeller types from multiple aspects, making it a potential candidate for further research and the development of a prototype for mechanized shrimp harvesting.

* Corresponding author.
E-mail address: k.sangpradit@rmutt.ac.th (K. Sangpradit)

https://doi.org/10.34044/j.anres.2023.57.5.06

Introduction

In 2018, ASEAN countries were the major contributors to the white shrimp harvest, accounting for 35% of the global production (461,000 t), as reported by Miao and Wang (2020). The collection process is still predominantly dominated by traditional manual methods (Thoetrattanakia and Sangpradit, 2022). Although mechanized approaches, such as vacuum harvesters, have faced limitations (Maulaya and Herodian, 2013), studies on fish harvesters have displayed potential for smaller-sized shrimp. However, they have not conformed to the usual consumption standards (Ohs et al., 2006). Researchers have been dedicated to resolving this challenge by concentrating on the development of adequate harvesting tools for white shrimp, with consideration of biomechanics (Jimenez et al., 2021).

Related research in the field of shrimp harvesting has emphasized the need for appropriate harvesting tools to meet specific criteria. One promising approach being explored was the use of a centrifugal pump technique for white shrimp harvesting, ensuring a force below 1.18 kg and a pressure below 160,000 Pa on the shrimp's body. The target transport rate was 9 kg/m^3, with a goal of achieving a harvest rate of 1,000 kg/hr (Thoetrattanakia and Sangpradit, 2022). To meet these requirements, researchers considered a finless impeller design. The numerical simulation adhered to the standards of SolidWorks Premium 2019 SP01 Flow Professional, using Cartesian-based meshes and Meshing Technology (Sobachkin and Dumnov, 2014). The analysis considered both laminar and turbulent flow conditions. This simulation setup ensured accurate and reliable results for studying the white shrimp harvesting process (Knudson, 2007; Alam et al., 2023).

The current study's main objective was to develop and assess the effectiveness of a centrifugal pump technique featuring a finless impeller design for the purpose of white shrimp harvesting. The primary goal was to optimize the flow rate and pressure distribution within the shrimp harvester pump housing, ensuring that the force and pressure applied to the white shrimp was maintained within acceptable limits. To achieve this, the research applied numerical simulations with SolidWorks Premium 2019 SP01 Flow Professional, using Cartesian-based meshes and Meshing Technology. These simulations accurately modeled and analyzed the white shrimp harvesting process (Knudson, 2007; Alam et al., 2023). The comprehensive investigation of various impeller models at different rotational speeds aimed to identify the most suitable impeller design for achieving efficient and sustainable white shrimp harvesting.

Material and Methods

The experimental field was located in the Wang Noi District, Phra Nakhon Si Ayutthaya Province, Thailand (14.207844993525049 N, 100.66707456856373E). The primary measuring tools and equipment were: 1) an Inverter (Mitsubishi Electric, A800 FR-A840-22K-1, serial number K08857001), with the main motor drive being an induction motor (22 KW 6 pole, type SF-JV, manufactured by Mitsubishi Electric Automation (Thailand), serial number A16); 2) a vacuum pump (ENVA Liquid Ring, Model 1EN015-03, S/N 2025450) accompanied by a vacuum motor (ABB Germany, Model M2BAX90SA2, S/N 8G1020360777864001); and 3) A clamp meter (FLUKE 325, serial number 463198MV); and (4) an ultrasonic flow meter (manufactured by IMARI, Japan, Model CLM-700, S/N 200323-H-81979116).

Numerical simulation method

Th numerical simulation method focused on the white shrimp harvester, specifically utilizing the centrifugal pump technique. The simulation involved the impeller and was conducted using the SolidWorks program (Solid work Premium 2019 SP1.0 Serial No. 9000 0119 3109 0543 H87B FQB8). This process leads to the division of the pump's grid domain and the impeller's grid (Fig. 1). A detailed breakdown of the number of cells can be found in Table 1. Essential data was obtained through simulation analysis, encompassing the flow rate for each impeller type, the corresponding pump head value and the pressure within the pump housing. The simulation considered the positioning of white shrimp at nine different locations within the pump house (Fig. 6 and Table 3). The speed of each impeller type was carefully adjusted within the range 240–300 revolutions per minute (RPM) to facilitate a comprehensive evaluation.

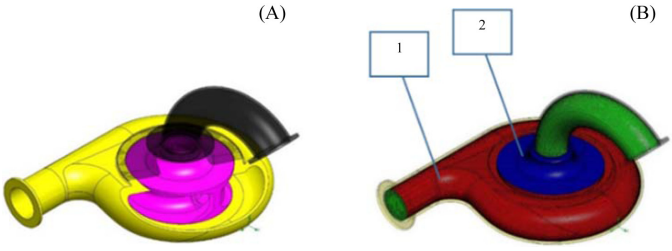

Fig. 1 (A) Impeller and shrimp harvester housing; (B) grid of computational domain for pump, where 1 = grid of housing and 2 = grid for impeller

Table 1 Geometrical parameters for impeller and housing of shrimp harvesting machine

Impeller type	Fluid cells	Solid cells	Partial cells	Total cells
Impeller IM1	634,356	300,016	156,153	1,090,525
Impeller IM2	645,542	308,382	161,427	1,115,351
Impeller IM3	547,508	302,150	144,962	994,620
Impeller IM4	558,164	303,246	148,703	1,010,113
Impeller IM5	594,806	307,522	154,588	1,056,916

Table 2 Test results for determining flow rate

Model IM3	240 RPM	255 RPM	270 RPM	285 RPM	300 RPM
IM3 simulation	17	351	425	571	715
IM3 actual	16.2	335.3	410	552.1	695.2
Difference	0.78	15.7	15	18.8	19.8
% Difference	4.6	4.47	3.5	3.3	2.8

RPM = revolutions per minute

Table 3 Shrimp position in system

Position	Area	Components
1	Suction inlet position	Inlet hose
2	Center position inside impeller,	Impeller
3	Positions inside impeller outlet mouth at No.1	Impeller
4	Positions inside impeller outlet mouth at No.2	Impeller
5	Positions inside pump housing at 0 degrees	Pump housing
6	Positions inside pump housing at 90 degrees	Pump housing
7	Positions within pump housing at 180	Pump housings
8	Positions inside pump housing at 270 degrees	Pump housing
9	Location inside pump housing at the outlet housing	Outlet pump housing

To ensure accuracy and reliability in the simulation, SolidWorks Premium 2019 SP01 Flow Professional (Solid work Premium 2019 SP1.0 Serial No. 9000 0119 3109 0543 H87B FQB8) was utilized, strictly adhering to its standard protocols. This advanced software played a crucial role in facilitating a detailed study of the white shrimp harvesting process within the centrifugal pump mechanism.

The simulation involved equations of mass, momentum and energy conservation to analyze the white shrimp harvester. Additionally, turbulent flow equations were utilized, specifically adopting the Standard k-ε turbulence model proposed by Sobachkin and Dumnov (2014). Notably, heat transfer analysis was not included in this particular study. In the fluid regions, SolidWorks Flow Simulation was applied to solve the Navier-Stokes equations, which were fundamental in describing the conservation laws for mass, momentum and energy (Equations 1–3). These equations are indispensable for understanding and analyzing the flow behavior and characteristics within the white shrimp harvester (Sobachkin and Dumnov, 2014).

By utilizing these numerical simulation methods and equations, this study aimed to gain insights into the performance and behavior of the white shrimp harvester during centrifugal pumping, thus facilitating a better understanding of its functionality and potential for enhancing white shrimp harvesting processes.

$$\frac{\partial \rho}{\partial t} + \frac{\partial (\rho u_i)}{\partial x_i} = 0 \quad (1)$$

$$\frac{\partial (\rho u_i)}{\partial t} + \frac{\partial}{\partial x_j}\left(\rho u_i u_j\right) + \frac{\partial P}{\partial x_i} = \frac{\partial}{\partial x_j}\left(\boldsymbol{\tau}_{ij} + \boldsymbol{\tau}_{ij}^{R}\right) + S_i \quad (2)$$

$$\frac{\partial \rho H}{\partial t} + \frac{\partial \rho u_i H}{\partial x_i} = \frac{\partial}{\partial x_i}\left(u_j\left(\tau_{ij} + \tau_{ij}^{R}\right) + q_i\right) + \frac{\partial \rho}{\partial t} - \tau_{ij}^{R}\frac{\partial u_i}{\partial x_i}\rho\varepsilon + S_i u_i + Q_H \quad (3)$$

$$H = h + \frac{u^2}{2}$$

where ρ = density of the fluid; t = time; u_j = velocity components in the i-direction; x_i = spatial coordinate components in the i-direction; τ_{ij} = viscous stress tensor; τ_{ij}^{R} = Reynolds stress tensor; S_i = body forces acting on the fluid; H = total enthalpy of the fluid; q_i = heat flux in the i-direction; ε = turbulence dissipation rate; and Q_H = the heat source/sink term.

The energy equations used for the calculation of high-speed compressible flows and flows with shock waves are presented in Equations 4–5:

$$\frac{\partial \rho E}{\partial t} + \frac{\partial \rho u_i\left(E + \frac{p}{\rho}\right)}{\partial x_i} = \frac{\partial}{\partial x_i}\left(u_j\left(\tau_{ij} + \tau_{ij}^{R}\right) + q_i\right) - \tau_{ij}^{R}\frac{\partial u_i}{\partial x_i}\rho\varepsilon + S_i u_i + Q_H \quad (4)$$

$$E = e + \frac{u^2}{2} \quad (5)$$

where E = total energy of the fluid; p = pressure of the fluid.

The modified k-ε turbulence model with damping functions, proposed by Lam and Bremhorst (1981), describes laminar, turbulent and transitional flows of homogeneous fluids, consisting of the following turbulence conservation laws as represented in Equations 6 and 7:

$$\frac{\partial \rho k}{\partial t} + \frac{\partial \rho k u_i}{\partial x_i} = \frac{\partial}{\partial x_i}\left(\left(\mu + \frac{\mu_t}{\sigma_k}\right)\frac{\partial k}{\partial x_i}\right) + \boldsymbol{\tau}_{ij}^R \frac{\partial u_i}{\partial x_i} - \rho\varepsilon + \mu_t P_B, \quad (6)$$

$$\frac{\partial \rho \varepsilon}{\partial t} + \frac{\partial \rho \varepsilon u_i}{\partial x_i} = \frac{\partial}{\partial x_i}\left(\left(\mu + \frac{\mu_t}{\partial \varepsilon}\right)\frac{\partial \varepsilon}{\partial x_i}\right) + C_{\varepsilon 1}\frac{\varepsilon}{k}\left(f_1 \boldsymbol{\tau}_{ij}^R \frac{\partial u_i}{\partial x_i} + C_B \mu_t P_B\right) - f_2 C_{\varepsilon 2}\frac{\rho \varepsilon^2}{k} \quad (7)$$

where k = turbulence kinetic energy; μ = dynamic viscosity; μ_t = turbulent viscosity; σ_k = turbulence model constants; and $C_{\varepsilon 1}$, $C_{\varepsilon 2}$, C_B, f_1, f_2 = turbulence model constants.

The relationships among the viscous stress tensor, the Reynolds stress tensor, the dynamic viscosity, the turbulent viscosity, the density of the fluid and the turbulence kinetic energy can be described using Equations 8 and 9.

$$\tau_{ij} = \mu s_{ij}, \tau_{ij}^R = \mu_t s_{ij} - \frac{2}{3}\rho k \delta_{ij} \; s_{ij} = \frac{\partial u_i}{\partial x_j} + \frac{\partial u_j}{\partial x_i} - \frac{2}{3}\delta_{ij}\frac{\partial u_k}{\partial x_k}, \quad (8)$$

$$P_B = \frac{g_i}{\sigma_B}\frac{1}{\rho}\frac{\partial \rho}{\partial x_i}, \quad (9)$$

where τ_{ij} = viscous stress tensor; τ_{ij}^R = Reynolds stress tensor; μ = dynamic viscosity; μ_t = turbulent viscosity; ρ = density of the fluid; k = turbulence kinetic energy; g_i = gravitational acceleration components in the i-direction; σ_B = turbulence model constant for buoyancy effects; and δ_{ij} = Kronecker delta.

Centrifugal force in bladeless shrimp harvesters

The primary aim of this study was to model and explain the concept of centrifugal force in a bladeless shrimp harvester. To fully grasp this concept, it was essential to have a fundamental understanding of centrifugal force. This paper emphasized the significant of centrifugal pumps and turbines across various engineering applications.

The centrifugal pump head formula represented by Equation 10, played a pivotal role:

$$H = \frac{(P_{dis} - P_{su})}{\rho g} + \frac{(V_{dis}^2 - V_{su}^2)}{2g} + Z_{dis} - Z_{su} \quad (10)$$

where: H = pump head; P_{dis} = pressure at the discharge; P_{su} = pressure at the suction; ρ = fluid density; g = acceleration due to gravity; V_{dis} = velocity at the discharge; V_{su} = velocity at the suction; Z_{dis} = elevation at the discharge; and Z_{dis} = elevation at the suction.

Similarly, for turbines, the turbine power output formula can be expressed using Equation 11:

$$P_{out} = \dot{m} \cdot H \cdot \eta_{turb} \quad (11)$$

where: P_{out} = turbine power output; $\dot{m}$ = mass flow rate; H = head developed by the turbine; and η_{turb} = turbine efficiency.

Furthermore, it is crucial to enhance the operational stability, efficiency and service life of centrifugal pumps to achieve improved energy efficiency and meet global carbon neutrality targets (Cong et al., 2015; Pei et al., 2017). Extensive research has been conducted on the relationship between energy loss and entropy generation in fluid machinery, thereby providing valuable insights for optimizing pump performance (Jiang et al., 2011; Fan et al., 2022; Lai et al., 2022; Zhang and Tang, 2022).

Experimental system

The experimental arrangement (Figs. 2A and 2B) comprised an inlet pipe, an impeller, a pump housing and a pump housing outlet pipe. To assess the system, the impeller was operated at rotational speeds of 240, 255, 270, 285 and 300 RPM. The experiment utilized five distinct propellers, denoted as IM1, IM2, IM3, IM4 and IM5, as depicted in Figs. 7–9. To facilitate comparison, data from simulations were exchanged to obtain various data points. The rotational speeds were deliberately selected to ensure safety and compatibility with the 30 HP motor.

The first step involved simulation using a program to determine the head pump flow rate and pressure at nine different positions within the pump housing. This simulation incorporated a model of the shrimp inside the pump housing to

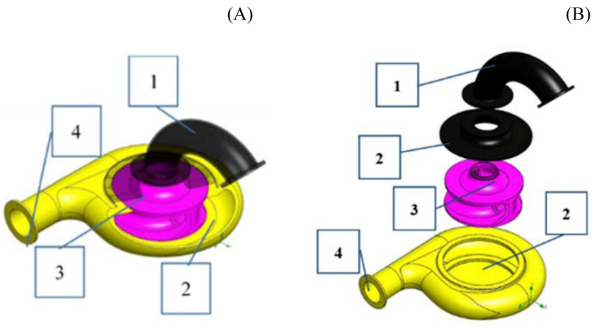

Fig. 2 (A) Shrimp harvester components; (B) internal components of the shrimp harvester, where 1 = inlet pipe, 2 = pump housing, 3 = impeller and 4 = outlet pipe

ascertain the pressure exerted on the shrimp (Table 3). Further experimental details are provided in Table 4. In the second step, the obtained simulation values were analyzed using statistical methods, such as comparative analysis, involving Tukey's HSD (honestly significant difference) test. These analyses were used to ascertain whether significant differences existed for each impeller. The third step verified the accuracy of the simulation by constructing a 254 mm shrimp harvester prototype and developing a prototype propeller, namely, IM3 (Figs. 3A and 3B). IM3, a small machine approximately 50 mm in size, is commonly used for transporting small fish. In the validation, the water flow rate was measured using the ultrasonic flow meter. The shrimp harvester housing incorporated essential electrical components, such as the main motor drive, the vacuum pump and measuring equipment, such as the clamp meter. Additionally, the inverter controlled the impeller speed of the prototype (2K-1).

The decision to use the IM3 impeller was driven by its fundamental design, its wide used in the conveyance of small fish and it being a technique highly appreciated and preferred by small-fish transporters. The primary aim of this study was to enhance the potential effectiveness of the shrimp harvesting process by adopting this impeller and incorporating established field practices and academic knowledge.

Pressure and flow rate

The current phase of this study involved conducting a simulation of the shrimp harvester (see Figs.1 and 2) to measure and evaluate its performance parameters. The primary objectives involved determining the water flow rate in units of cubic meters per hour, as shown in Fig. 11, assessing the pump head (in meters of water), as shown in Fig. 13 and analyzing nine pressure values (in pascal) acting on the white shrimp (Fig. 6 and Table 3). Upon acquiring the requisite data, the accuracy of the centrifugal pump with a 254 mm diameter was verified. An inverter was used to regulate the rotational speed, enabling the development of prototypes that faithfully represented real-world operating conditions.

Analysis of variance and Tukey's honest significant difference impeller models

The statistical analysis, based on Tables 8–9, applied Tukey HSD test to assess the flow rate and pressure variations among the different impeller models for white shrimp harvesting. Table 8 presents the Tukey HSD results for the flow rate and revealed noteworthy differences in the flow rates between the impeller models (IM1, IM2, IM3, IM4 and IM5) at various RPMs. Specifically, IM1 displayed significant deviations from the other models, indicating its suitability for achieving the desired flow rates. Statistically significant distinctions were observed between IM2 and IM3, IM2 and IM4 and IM3 and IM4. However, no noteworthy disparities were found between IM2 and IM5, nor between IM3 and IM5.

Table 9, presents Tukey's HSD post-hoc test results for pressure, indicating that impeller model IM1 surpassed the other models in pressure generation for white shrimp harvesting. The analysis of variance test demonstrated considerable variations in pressure values among the impeller models and RPM settings. The post-hoc analysis further confirmed IM1's superiority, showing significant pressure differences compared to specific RPM pairs and other impeller models.

Verification of the simulated model

The primary objective of this study was to validate the design of the shrimp harvester by incorporating a finned impeller adhering to a standard centrifugal pump. To achieve this goal, a tangible prototype was manufactured of the harvester (labeled as IM3), featuring a 254 millimeter diameter,

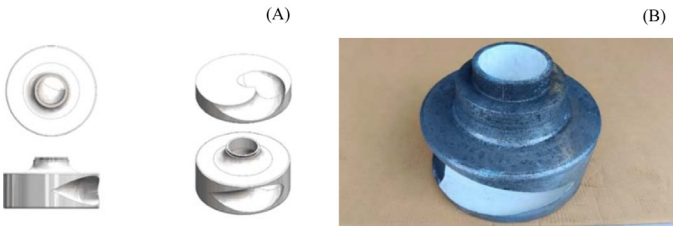

Fig. 3 Impeller model IM3 (size 254 mm): (A) drawing; (B) real model

Table 4 Experimental design

Impeller type	240 RPM	255 RPM	270 RPM	285 RPM	300 RPM
IM1	X Y Z	X Y Z	X Y Z	X Y Z	X Y Z
IM2	X Y Z	X Y Z	X Y Z	X Y Z	X Y Z
IM3	X Y Z	X Y Z	X Y Z	X Y Z	X Y Z
IM4	X Y Z	X Y Z	X Y Z	X Y Z	X Y Z
IM5	X Y Z	X Y Z	X Y Z	X Y Z	X Y Z

X = flow rate; Y = head pump; Z = pressure acting on the shrimp; RPM = revolutions per minute

(Fig. 4), with the impeller (Fig. 3). Subsequently, the flow rates were evaluated at various revolution speeds (240, 255, 270, 285 and 300 RPM), as shown in Figs. 5A and 5B. The selection of the IM3 impeller was based on its fundamental design, which significantly enhanced the harvester's performance, as elaborated in the Experimental System section.

The simulation model was crucial in accurately representing the design of the finned impeller, encompassing the specified inlet and outlet angles. By simulating flow behavior at these speeds, the model provides valuable insights into expected flow rates and the overall performance of the harvester (Figs. 12–13). To validate the model, a comparison between simulated flow rates and corresponding experimental data is essential. This step ensures the simulation's accuracy and alignment with the observed performance of the finned impeller at different speeds.

Five different impeller edge designs were manufactured for the experiment. Each impeller featured a distinct geometric shape and exit configuration. IM1 and IM2 had a rectangular geometrical shape inside, with 2 and 3 exits, respectively. IM3, IM4 and IM5 had a cavity inside with a circular geometrical shape and 1, 2 and 3 exits, respectively, as shown in Figs. 4–7. These propellers were utilized in the experiment and their performance was evaluated by measuring flow rates at various speeds of 240, 255, 270, 285 and 300 RPM.

Fig. 4 Shrimp harvesting machine with impeller model IM3 (size 254 mm)

Fig. 5 (A) Shrimp harvesting machine; (B) running shrimp harvesting to determine flow rate

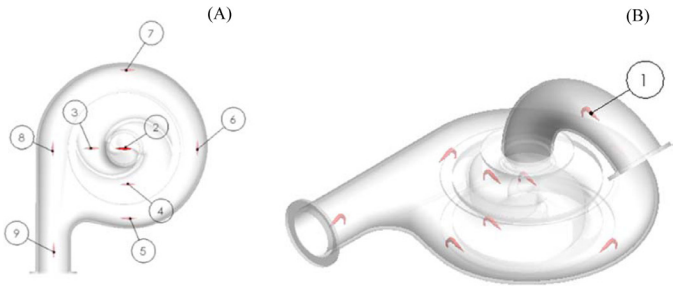

Fig. 6 Nine placement locations in white shrimp system: (A) top view; (B) isometric view

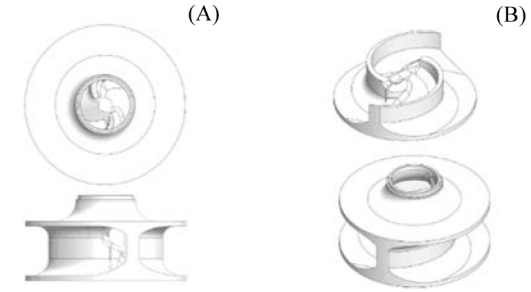

Fig. 7 Impeller IM1 top side views (A); isometric views (B)

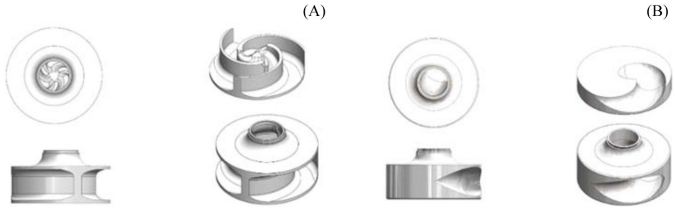

Fig. 8 Top, side, isometric and section views: (A) impeller IM2; (B) impeller IM3

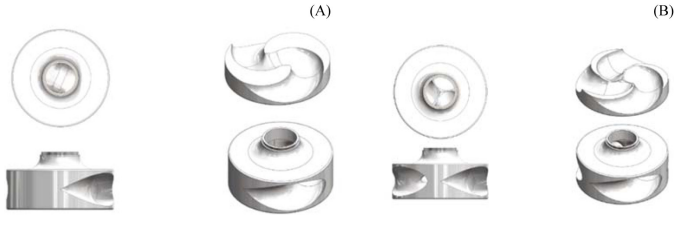

Fig. 9 Top, side, isometric and section views: (A) impeller IM4; (B) impeller IM5

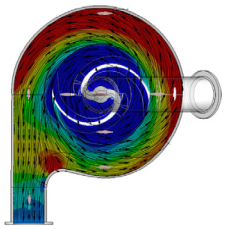

Fig. 10 Static pressure distributions in shrimp harvest machine at 300 revolutions per minute based on impeller model IM1 blue represents 135,822.1 Pascal near the blades, and the highest pressure, in red, is 152,983.74 Pascal

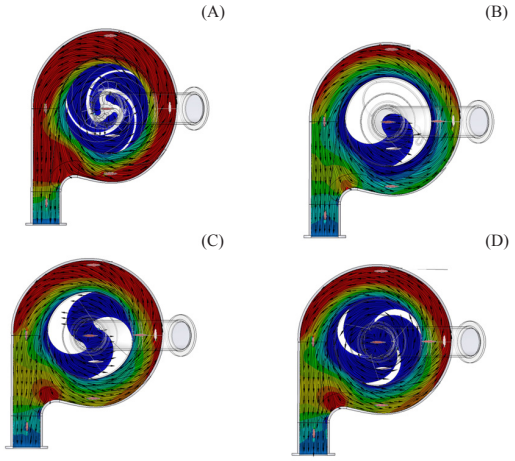

Fig. 11 Static pressure distributions in shrimp harvest machine at 300 revolutions per minute for impeller models: (A) IM2; (B) IM3; (C) IM4; (D) IM5 blue represents 135,822.1 Pascal near the blades, and the highest pressure, in red, is 152,983.74 Pascal

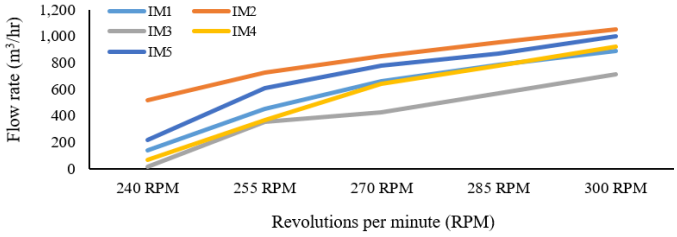

Fig. 12 Comparative performance of impeller models based on flow rate at different revolutions per minute

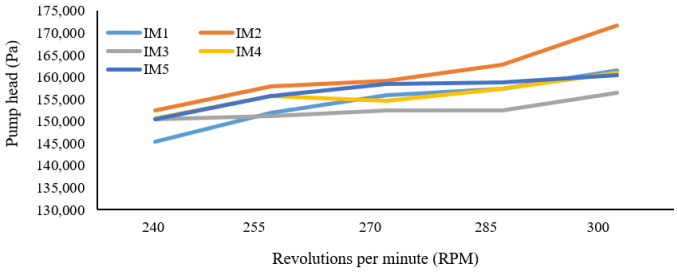

Fig. 13 Variation in pump head for different impeller models with revolutions per minute

The experiment focused on the following key measurements and analyses: (1) pump head by evaluating the pressure or energy imparted by the pump to the fluid, indicating its capacity to move the fluid through the system; (2) flow rate by quantifying the volume of fluid passing through the system per unit of time, commonly measured in m^3/h or an appropriate unit; (3) pump housing pressure distribution, by examining pressure variations at different locations within the pump housing; and (4) shrimp pressure, by measuring the pressure exerted on the shrimp at various positions in the system, allowing for the assessment of potential impacts during the harvesting process.

These measurements were conducted at nine positions within the system. Through data analysis at each position and its correlation with propeller speed, valuable insights were gained regarding the performance of the different propellers and their suitability for efficient shrimp harvesting.

Results and Discussion

Numerical simulation pressure and flow rate.

The experiment conducted on the shrimp harvester focused on analyzing the flow rate and pressure distribution of different centrifugal pump designs, involving five distinct impeller models. Measurements were taken at nine different positions within the harvester to assess the performance of each impeller at various RPMs.

The findings revealed that each impeller model exhibited different flow rates and pressures at distinct RPMs. Impeller model 1 (IM1) displayed flow rates ranging from 138 m3/hr at 240 RPM to 886 m^3/hr at 300 RPM (Table 5 and Fig. 12). The corresponding minimum and maximum head pressures recorded were 145,374 Pa and 161,637 Pa, respectively (Table 6 and Fig. 13). Similarly, impeller model 2 (IM2) demonstrated flow rates ranging from less than 240 m^3/hr at 240 RPM to a maximum of 519 m^3/hr at 300 RPM, with minimum and maximum associated head pressures of 152,464 Pa and 171,660 Pa, respectively. For impeller model 3 (IM3), the flow rate ranged from 17 m^3/hr at 240 RPM to a maximum of 715 m^3/hr . at 300 RPM, with corresponding minimum and maximum head pressures of 150,460 Pa and 156,398 Pa, respectively. Impeller model 4 (IM4) produced a flow rate of 64 m^3/hr at 240 RPM and achieved a maximum flow rate of 921 m^3/hr at 300 RPM, with recorded minimum and maximum head pressures of 150,658 Pa and 161,020 Pa, respectively. Finally, impeller model 5 (IM5) produced flow rates ranging from 216 m^3/hr at 240 RPM to 1,001 m^3/hr at 300 RPM, with minimum and maximum head pressures of 150,541 Pa and 160,511 Pa, respectively.

Table 5 Simulation results of flow rate (m^3/hr)

Impeller type	240 RPM	255 RPM	270 RPM	285 RPM	300 RPM
IM1	138	449	657	781	886
IM2	519	728	849	956	1053
IM3	17	351	425	571	715
IM4	64	364	642	775	921
IM5	216	607	774	866	1001

RPM = revolutions per minute

Table 6 Pressure simulation results (Pa)

Impeller type	240 RPM	255 RPM	270 RPM	285 RPM	300 RPM
IM1	145,374	152,006	155,852	157,338	161,637
IM2	152,464	157,954	159,264	162,864	171,660
IM3	150,460	151,132	152,515	152,533	156,398
IM4	150,658	155,788	154,630	157,443	161,020
IM5	150,541	155,716	158,536	158,816	160,511

RPM = revolutions per minute

Table 7 Simulation results for pressure applied to white shrimp body at 9 positions (pascal) for different impellers (IM 1, IM2, IM3, IM4, IM5)

Rotational speed (RPM)	Shrimp Position 1	Shrimp Position 2	Shrimp Position 3	Shrimp Position 4	Shrimp Position 5	Shrimp Position 6	Shrimp Position 7	Shrimp Position 8	Shrimp Position 9
IM1									
240	88,370	84,848	112,561	113,816	130,320	136,850	147,470	141,212	140,256
255	86,800	86,032	114,142	146,573	139,466	145,218	157,401	145,543	142,374
270	84,419	86,086	117,176	120,243	145,583	149,264	157,864	149,715	145,626
285	82,181	84,139	119,853	121,418	146,910	151,544	161,114	152,371	146,244
300	80,056	82,960	121,509	125,327	150,424	155,742	162,664	153,467	149,291
IM2									
240	86,075	86,542	110,005	118,531	140,759	146,256	158,399	146,370	143,753
255	83,084	85,896	113,882	122,249	146,091	152,734	160,821	152,170	147,260
270	81,082	85,777	117,486	124,116	149,956	153,773	161,652	153,457	148,242
285	78,539	83,564	118,277	124,795	153,253	155,677	164,560	154,066	150,499
300	80,056	82,960	121,509	125,327	150,424	155,742	162,664	153,467	149,291
IM3									
240	89,289	88,672	107,902	120,915	136,091	142,648	152,204	144,715	139,476
255	88,037	87,735	109,675	122,923	139,323	143,123	155,515	145,755	141,884
270	87,289	86,891	110,982	125,622	144,644	145,376	156,692	147,053	142,289
285	85,568	86,172	111,013	128,578	141,270	146,110	156,200	149,180	143,012
300	83,370	85,564	111,686	130,845	145,392	148,269	158,011	149,460	146,286
IM4									
240	89,747	90,336	108,312	122,064	138,070	142,643	152,370	146,502	143,082
255	87,188	87,054	108,060	121,582	144,131	147,506	157,836	149,129	144,457
270	84,619	85,968	109,093	124,073	144,100	148,698	158,602	148,950	144,130
285	82,291	83,679	108,648	124,795	146,692	150,060	158,446	150,961	148,021
300	79,335	81,585	108,502	125,646	150,170	154,863	162,522	154,281	150,121
IM5									
240	89,520	91,635	104,872	117,520	140,309	142,706	155,042	146,709	143,082
255	85,179	86,952	97,320	112,772	144,050	149,832	160,815	148,697	144,055
270	82,368	84,657	92,327	117,525	148,656	151,773	161,691	152,096	147,057
285	80,428	82,827	90,963	116,301	149,715	151,582	160,714	151,504	149,565
300	77,528	81,275	89,539	119,696	150,296	155,598	162,726	155,613	151,702

RPM = round per minute

Analysis of variance and Tukey's HSD

Based on the statistical analysis, the following conclusions were drawn:

(1) flow rate (Table 8): among the different impeller models, IM1 consistently demonstrated the highest flow rates across various RPM settings, indicating its superior performance compared to the other models in terms of fluid flow efficiency;

(2) pressure (Table 9): impeller models IM1 and IM3 consistently exhibited the highest-pressure values at different RPM settings, establishing them as the top-performing impeller models in terms of pressure generation within the shrimp harvester pump housing.

Table 8 Results for Tukey's honestly significant difference test for flow rate

Group1	Group2	µdif	*p*-adj*	Lower	Upper	Reject
IM1	IM2	366.4	0.001	265.1	467.7	TRUE
IM1	IM3	321.8	0.001	220.5	423.1	TRUE
IM1	IM4	280.2	0.001	178.9	381.5	TRUE
IM1	IM5	397.0	0.001	295.7	498.3	TRUE
IM2	IM3	-44.6	0.001	-145.9	-43.3	TRUE
IM2	IM4	-86.2	0.001	-187.5	-84.9	TRUE
IM2	IM5	30.6	0.001	-70.7	132.9	FALSE
IM3	IM4	-41.6	0.001	-142.9	-40.3	TRUE
IM3	IM5	75.2	0.001	-26.1	176.5	FALSE
IM4	IM5	116.8	0.001	15.5	218.1	TRUE

* = *p*-adjusted value < 0.05; µdif = difference

Table 9 Significant pairs based on Tukey's honestly significant difference post-hoc test for pressure

Impeller model	Significant RPM pairs	*p* Value*
IM1	240 RPM - 270 RPM	< 0.05
	240 RPM - 285 RPM	< 0.05
	240 RPM - 300 RPM	< 0.05
	255 RPM - 300 RPM	< 0.05
IM2	240 RPM - 300 RPM	< 0.05
IM3	None	N/A
IM4	None	N/A
IM5	240 RPM - 255 RPM	< 0.05
	240 RPM - 285 RPM	< 0.05
	255 RPM - 300 RPM	< 0.05
	270 RPM - 300 RPM	< 0.05

RPM = revolutions per minute; * = *p* value < 0.05

Pressure distribution in shrimp harvester pump housing

The pressure measurements were conducted at nine specific points within the shrimp harvester pump housing, including positions at the suction inlet, impeller midpoint and exits of IM1 and IM2. Additionally, positions at 90 degrees, 180 degrees, 270 degrees and an additional 270-degree position were considered for analysis.

At Position 7 (located at 180 degrees inside the pump housing), with the impeller rotating at 300 RPM, the study recorded the maximum pressure values for each impeller model as: IM1reached a maximum pressure of 162,664 Pa at 300 RPM; IM2 also attained a maximum pressure of 162,664 Pa at 300 RPM; IM3 produced a maximum pressure of 162,664 Pa at 300 RPM; IM4 generated a maximum pressure of 158,011 Pa at 300 RPM and; IM5 produced the highest recorded pressure of 162,726 Pa at 300 RPM.

These results represented the maximum pressure values obtained at Position 7 within the shrimp harvester pump housing when the impeller was operating at its highest speed of 300 RPM. While there were slight variations among the impeller models, the IM5 impeller achieved the highest recorded pressure (Table 7 and Fig. 14).

Simulation model verification

A comparative analysis was conducted using the propeller prototype IM3 to rigorously validate the simulation model. The simulation projected a remarkable water flow rate of 17,351,435,571,715 m^3/hr. Subsequently, real-world trials and prototypes were tested and the actual water flow rates were measured at propeller speeds of 240, 255, 270, 285 and 300 RPM, yielding values of 16.2, 335.3, 410, 552.1 and 692.2 m^3/hr, respectively. The level of precision achieved in the comparison of the simulation and actual trials was an impressive 96.26% (Table 2). Notably, the simulation's precision was even higher when the rotational velocity was increased, particularly up to 285 RPM. These findings accentuated the dependability and strength of our simulation model, providing valuable insights for potential improvement, particularly at higher propeller velocities.

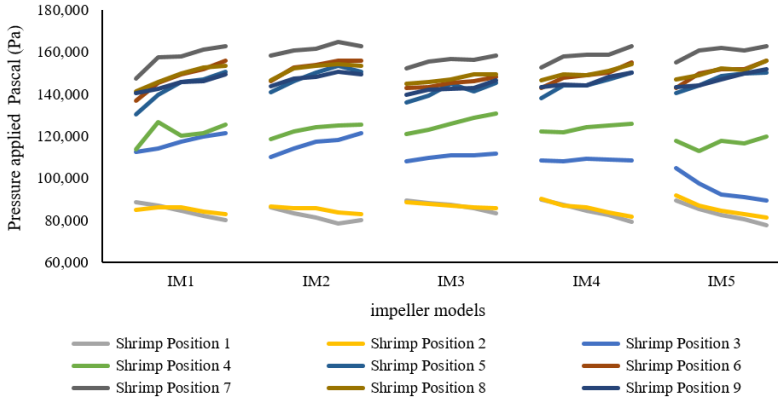

Fig. 14 Simulation results for pressure applied to white shrimp body at nine positions for different impeller models (IM 1, IM2, IM3, IM4 and IM5)

Comprehensive analysis of factors in shrimp harvester pump housing

After considering factors such as water flow rate, maximum pressure and impact on the shrimp, the design of the propeller for the white shrimp harvester prototype was prioritized for large inlet and outlet sizes to minimize damage to the harvested shrimp. Among the propellers evaluated, IM1 and IM3 were deemed more suitable due to their larger openings.

It was observed that the IM1, IM2 and IM5 propellers produced sufficient flow rates. However, IM3 had a low flow rate of 17 m^3/hr, which was not efficient for white shrimp harvesting, especially considering standard white shrimp pond sizes. Furthermore, while IM2 and IM3 could generate higher flow rates, they were less adaptable compared to IM1. In terms of pressure, all propeller types (IM1, IM2, IM3, IM4 and IM5) generated similar pressure levels. The highest-pressure point in the harvester was observed at Position 7 with the impeller rotating at 300 RPM. Both the IM1 and IM3 propellers met the pressure requirements. However, IM1, with its higher flow rate, was a more suitable choice for further development as a practical prototype (Table 7 and Fig. 14).

The study determined that that 270 RPM was the optimal rotational speed for evaluating properties, especially water flow rate. Operating the IM1 impeller at this speed minimized the risk of damaging the white shrimp body. In addition, at 270 RPM, the pressure exerted on the white shrimp reached its highest value of 157,864 Pa, indicating the effectiveness of this rotational speed in the white shrimp harvesting process.

Conclusion

The statistical analysis revealed that the impeller models IM1 and IM3 had superior performance in both flow rate and pressure generation. Throughout the white shrimp harvester experiment, these models consistently demonstrated the most promising results. As a result, IM1 and IM3 were deemed the most suitable choices for further development and implementation in a white shrimp harvester prototype.

Based on the study findings, it was concluded that the IM1 impeller, operating at a rotational speed of 270 RPM, was the optimal choice for developing a white shrimp harvester prototype. At this specific rotational speed, the IM1 impeller not only generated the maximum pressure acting on the shrimp, particularly at Position 7 (157,864 Pa), but also achieved a significantly different flow rate of 657 m^3/hr. These results underscored the effectiveness of the IM1 impeller at this particular rotational speed for successful white shrimp harvesting. The study's robust analysis and evaluation should provide valuable guidance for the design and implementation of a white shrimp harvester, enhancing its potential effectiveness in practical applications.

Conflict of Interest

The authors declare that there are no conflicts of interest.

References

Alam, S.M., Michael, P., Lin, C.K. 2003. Shrimp harvesting technology on the south west coast of Bangladesh. Aquaculture Asia 8: 29–30.

Cong, X., Zhou, R., Han, Y., Zhang, F., Chen, L. 2015. Optimization design of deep-well centrifugal pump based on CFX orthogonal test. Fluid Mach. 43: 22–25.

Fan, B., Liang, Z., Fan, R., Chen, S. 2022. Numerical study on entropy generation of the multi-stage centrifugal pump. Entropy 24: 923. doi.org/10.3390/e24070923

Jiang, J., Wang, R., Pezeril, M., Wang, Q.A. 2011. Application of varentropy as a measure of probabilistic uncertainty for complex networks. Chin. Sci. Bull. 56: 3677–3682. doi.org/10.1007/s11434-011-4697-3

Jimenez, Y.E. Marsh, R.L. Brainerd, E.L. 2021. A biomechanical paradox in fish: swimming and suction feeding produce orthogonal strain gradients in the axial musculature. Sci Rep. 11: 10334. doi.org/10.1038/s41598-021-88828-x

Knudson, D. 2007. Fundamentals of Biomechanics, 2nd ed. Springer. Chico, CA, USA.

Lai, F., Huang, M., Wu, X., Nie, C., Li, G. 2022. Local entropy generation analysis for cavitation flow within a centrifugal pump. J. Fluids Eng. 144: 101206. doi.org/10.1115/1.4054467

Lam, C.K.G., Bremhorst, K. 1981. A modified form of the k-epsilon model for predicting wall turbulence. Transactions of the ASME 103: 456–460.

Maulaya, R., Herodian, S. 2013. Design of a vacum type shrimp *Penaeus* sp. harvester. Jurnal Keteknikan Pertanian 27: 19–26. doi.org/10.19028/jtep.27.1.19-26 [in Indonesian]

Miao, W., Wang, W. 2020. Trends of aquaculture production and trade: Carp, tilapia, and shrimp. In: Food and Agriculture Organization of the United Nations. Understanding Antimicrobial Resistance in Aquaculture. Asian Fisheries Society. Selangor, Malaysia pp. 1–10. doi: 10.33997/j.afs.2020.33.S1.001

Ohs, C.L., Grabe, S.W., Creswell, L. 2006. The utilization of a fish pump for harvesting shrimp from tanks and ponds. https://fisheries.tamu.edu/files/2013/09/The-Utilization-of-a-Fish-Pump-for-Harvesting-Shrimp-from-Tanks-and-Ponds.pdf, 23 February 2022.

Pei, J., Yi, T., Yuan, S., Wang, W., Wang, J. 2017. Cavitation optimization for a centrifugal pump impeller by using orthogonal design of experiment. Chin. J. Mech. Eng. 30: 103–109. doi:10.3901/cjme.2016.1024

Sobachkin, A., Dumnov, D. 2014. Numerical basis of CAD-embedded CFD. In: Proceedings of NAFEMS World Congress 2013. Salzburg, Austria, pp. 1–19.

Thoetrattanakia, S., Sangpradit, K. 2022. Effect of fluid velocity in piping system physical properties for shrimp harvesting. In: The 11th Rajamangala University of Technology International Conference. Pattaya, Thailand, pp. 86–96.

Zhang, X., Tang, F. 2022. Energy loss evaluation of axial flow pump systems in reverse power generation operations based on entropy production theory. Sci. Rep. 12: 8667. doi.org/10.1038/s41598-022-12667-7